

**Morphology controlled synthesis of monodispersed manganese
sulfide nanocrystals and their primary application for supercapacitor
with high performance**

Yongfu Tang*, Teng Chen, Shengxue Yu

Experimental Section

1. Synthesis of MnS nanocrystals

(A) **Hollow spindle-like MnS nanospheres** 0.3 g $\text{MnCl}_2 \cdot 4\text{H}_2\text{O}$ was dissolved in 50 ml deionized water. Then, 5 ml ammonia (25~28 wt.%) was added to the solution under vigorous stirring. After 20 min, 15 ml of 0.1 M Na_2S solution was dropwise added into the above suspension. Subsequently, the suspension was transferred into a 100 mL Teflon-lined stainless-steel autoclave to be heated at 130 °C for different times (20 min, 2 h, 5 h, 8 h, 12 h and 24 h). The samples, obtained after washing, filtering and drying, were denoted as HS-NSs MnS nanocrystals. Another sample was obtained with lower Na_2S solution concentration of 0.05 M to investigate the effect of sulfide ion content on the structure and morphology of the MnS nanocrystals.

(B) **Tetrapod branched MnS nanorods** The process was similar to that of HS-NSs MnS nanocrystals. The only difference was that the concentration of Na_2S solution is 0.2 M. The obtained sample was denoted as TP-NRs MnS nanocrystals.

(C) **Solid spindle-like $\text{Mn}(\text{OH})_2$ and Mn_3O_4 nanospheres** 0.3 g $\text{MnCl}_2 \cdot 4\text{H}_2\text{O}$ was dissolved in 50 ml distilled water, then added 5 ml ammonia (25~28 wt.%) to the solution under vigorous stirring. Subsequently, the obtained suspension was transferred into a 100 mL Teflon-lined stainless-steel autoclave to be heated at 130 °C

for 8 h. The sample is obtained after washing, filtering and drying. The Mn_3O_4 nanospheres with similar morphology to $\text{Mn}(\text{OH})_2$ were obtained after calcining the as-prepared $\text{Mn}(\text{OH})_2$ at 400 °C for 2 h.

(D) Floccules coated single MnS nanorods 0.3 g $\text{MnCl}_2 \cdot 4\text{H}_2\text{O}$ was dissolved in 50 ml distilled water, then added 15 ml of 0.1 M Na_2S solution under vigorous stirring. Subsequently, the obtained suspension was transferred into a 100mL Teflon-lined stainless-steel autoclave to be heated at 130 °C for 8 h. The sample is obtained after washing, filtering and drying.

(E) MnS nanocrystal obtained with thiourea as sulfide source The process is similar to that for obtaining the floccules coated single MnS nanorods above. Thiourea was used to substitute the Na_2S solution as sulfide source.

2. Physicochemical characterization of MnS nanocrystals.

X-ray diffraction (XRD) patterns were recorded using a Bruker AXS D8 diffractometer with Cu K Radiation ($\lambda = 0.15418$ nm) at 40 kV and 30 mA. The morphology and microstructure of the MnS nanocrystals were characterized by HT 7700 model transmission electron microscopy (TEM) and KYKY-2800B model field emission scanning electron microscope (FESEM). The crystal structure information of MnS nanocrystals were characterized by high-resolution transmission electron microscopy (HRTEM).

3. Preparation of working electrode and electrochemical measurements.

The working electrodes for cyclic voltammetry (CV), charge-discharge and electrochemical impedance spectroscopy (EIS) were prepared by mixing active

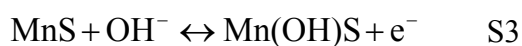
materials, acetylene black, and polytetrafluoroethylene (PTFE) at a weight ratio of 70:15:15, coating on nickel foam current collector, drying and pressing. The electrochemical measurements including CV and EIS were carried out via three-electrode system on CHI 660A workstation in 2.0 M KOH solution. The counter electrode and reference electrode are Pt foil (1 x 1 cm²) and Hg/HgO electrode, respectively. The charge-discharge measurements were performed by Land CT 2001A battery tester in 2.0 M KOH solution.

Supplementary Equations:



$$C = \int idV / v\Delta V \quad \text{S2}$$

where i is the mass current density, v is the potential scan rate, ΔV is the potential scan range (potential window) and dV is the differential of potential.



Discussion for Equation S3 and S4: As shown in **Figure 3a**, clear electrochemical redox peaks are present in the CV curve of the MnS TP-NRs electrode, indicating the valence change of manganese. For charging, due to the layered structure of wurtzite γ -phase MnS, the rich hydroxyl ions in electrolyte can be easily intercalated into the layers between the manganese ions and sulfide ions to balance the valence increase of manganese (**Equation S3**). With the continuously increasing of the overpotential, more hydroxyl ions are intercalated in the layers, along with the further valence increase of manganese to IV state (**Equation S4**). All the processes are reversed for

discharging. The proposed formation is clearly illustrated in **Figure 3e** and confirmed by the result that the specific capacitance of MnS TP-NRs with purer γ -phase structure is markedly higher than that of MnS HS-NSs with both α -phase and γ -phase structures.

Supplementary Figures:

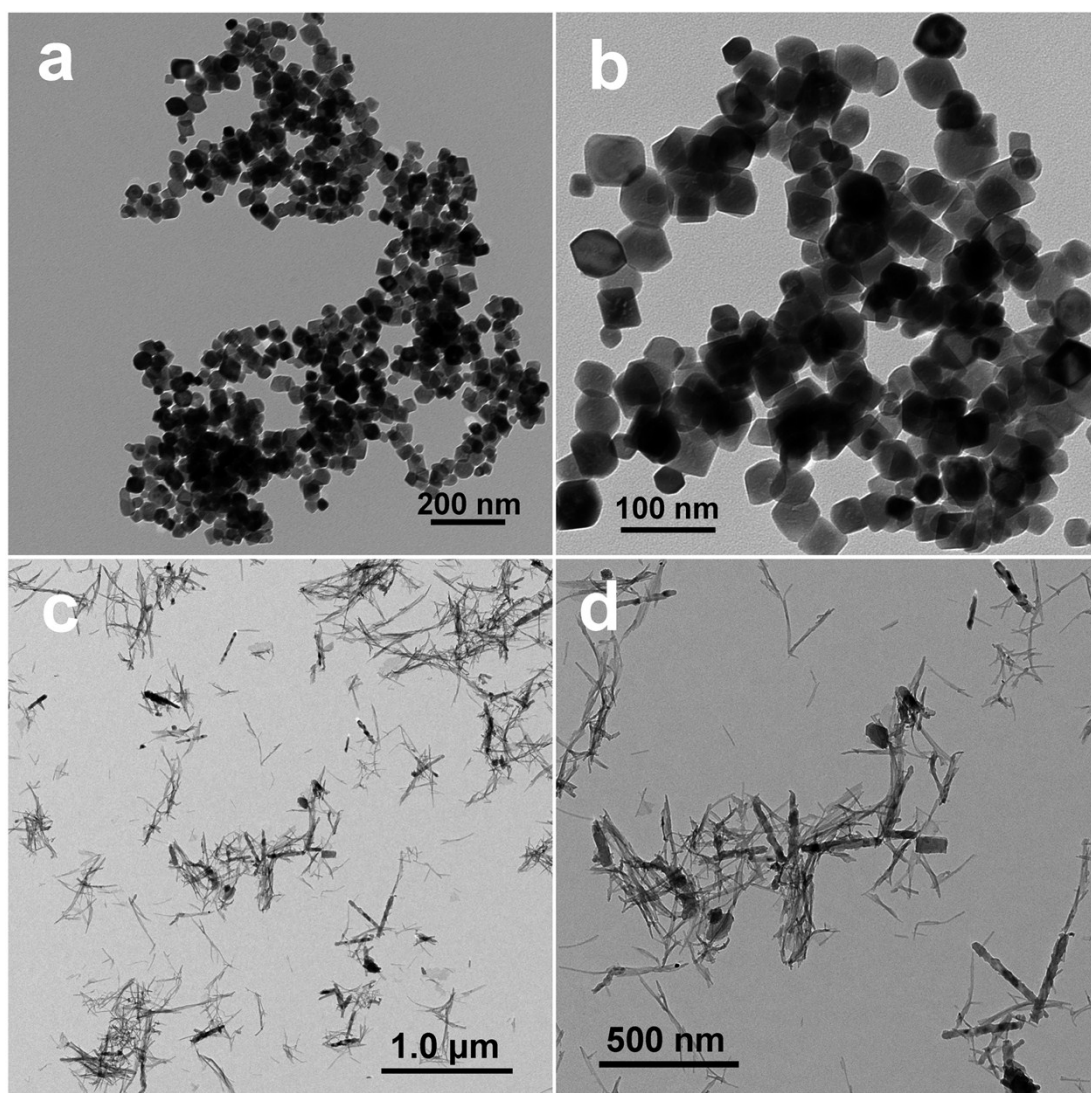


Figure S1. Low magnified (a), high magnified (b) TEM images of MnS nanocrystals obtained from the hydrothermal coprecipitation process without ammonia, and low magnified (c), high magnified (d) TEM images of Mn(OH)₂ nanocrystals obtained from the hydrothermal coprecipitation process with ammonia as precipitator

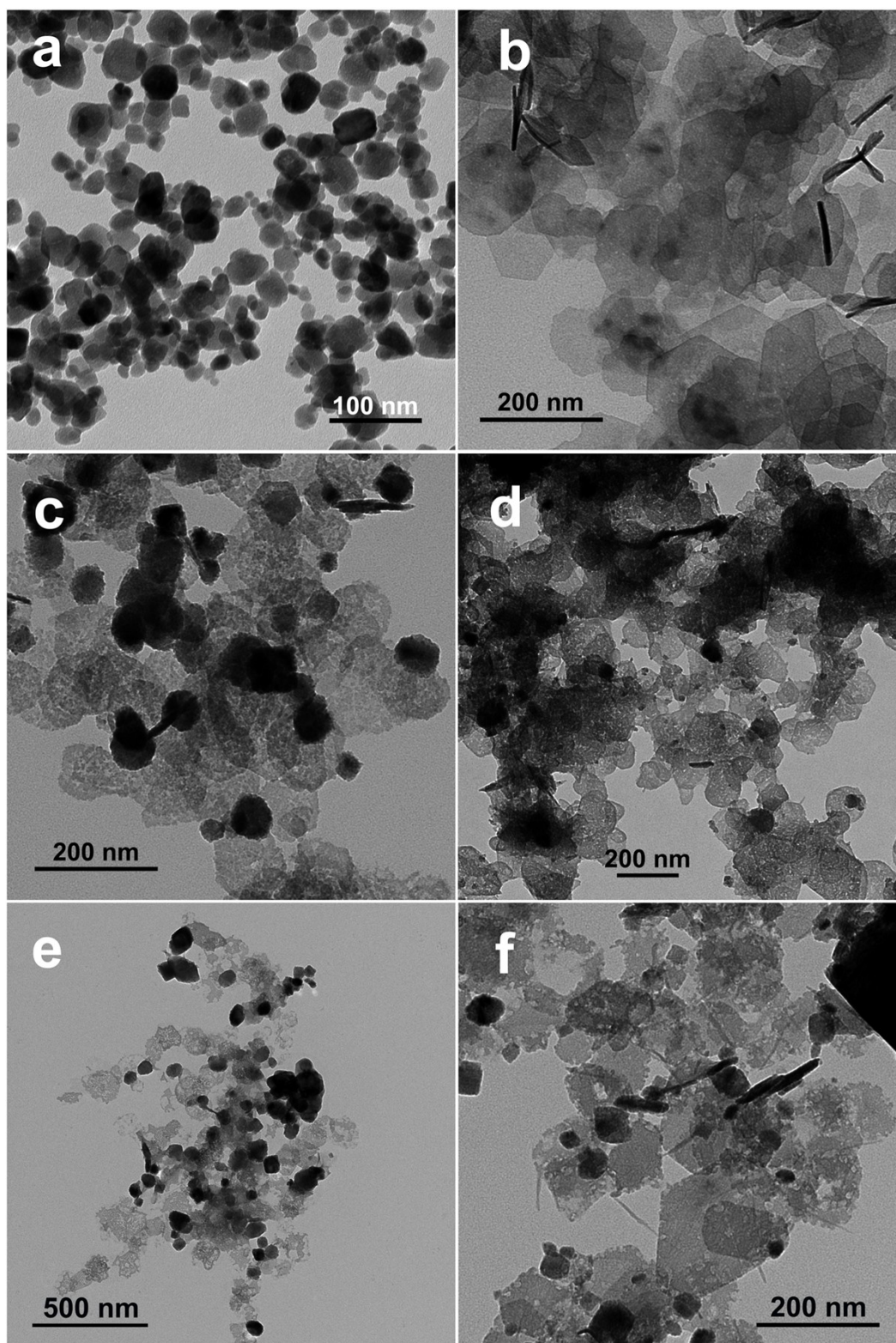


Figure S2. The HS-NSs nanocrystals obtained at 20 mins (a), 2 h (b), 5 h (c), 8 h (d), 12 h (e) and 24 h (f).

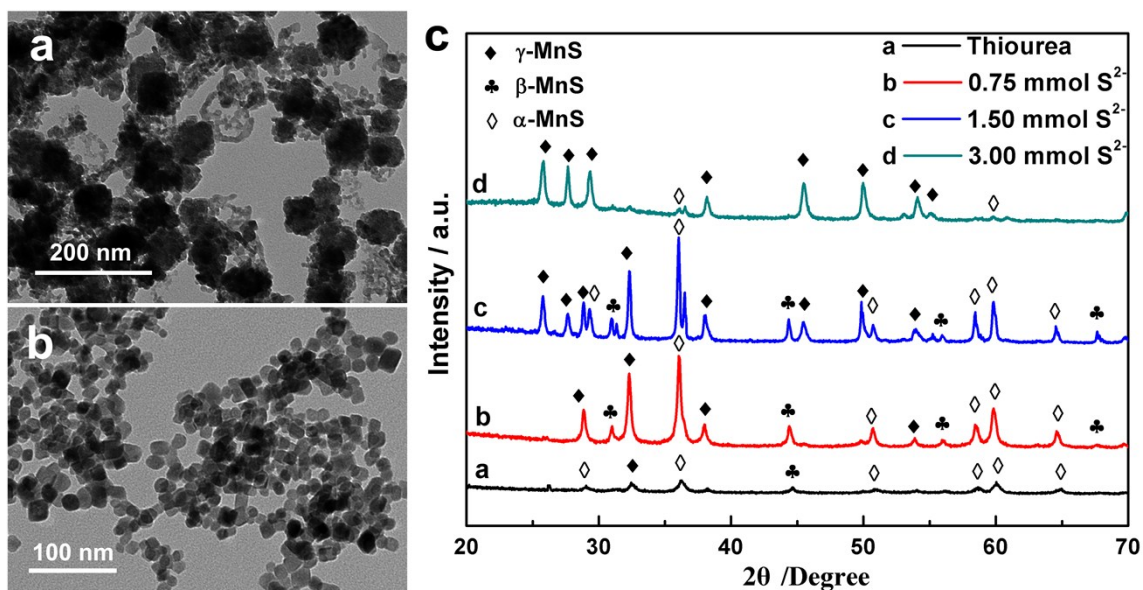


Figure S3. (a) MnS nanocrystals obtained via the similar process of the HS-NSs and TP-NRs but with the sulfide ion content of 0.75 mmol, (b) MnS nanocrystals obtained via hydrothermal process with thiourea as the sulfide source, (c) XRD patterns of the MnS nanocrystals obtained with different sulfide ion contents, as well as with thiourea as sulfide source.

Discussion: To further investigate the effect of sulfide ions on the structure and morphology of the MnS nanocrystals, another two MnS nanocrystals samples were synthesized for comparison with the HS-NSs and TP-NRs MnS nanocrystals. As shown in **Figure S3a**, when the sulfide ions content decreased to 0.75 mmol, collapsed hollow structure are observed in the images. This should be attributed to that the low content can not offer enough sulfide ions to substitute the hydroxyl ions lost during the further ion exchange process. Therefore, the holes become larger than that of HS-NSs based on the Kirkendall effect, and then collapse when framework was destroyed. When the thiourea is used as the sulfide sources, the sulfide releases slowly via the hydrolysis of thiourea, together with the production of ammonia to simulate the low sulfide ion content and the constant ratio (sulfide ion/ammonia = 2)

between the sulfide ion and ammonia. As shown in **Figure S3b**, solid spindle-like MnS nanospheres with the size of 20 nm, which is much smaller than that of HS-NSs (~100 nm), are obtained. The uniform hydrolysis of thiourea can offer much sulfide for the nucleation of MnS, which contributes the smaller size of MnS nanocrystals. XRD patterns of the MnS nanocrystals obtained with different sulfide ion contents (**Figure S3c**) also illustrate the effect of the sulfide ion content on the structure of the MnS nanocrystals. When the sulfide ion content was low or the thiourea was used as sulfide source, α -phase MnS tend to be obtained. By contrast, the sulfide ion content should be increased to gain the metastable γ -phase MnS. These results verify the formation mechanism of HS-NSs and TP-NRs MnS nanocrystals mentioned in the **Scheme 1**.

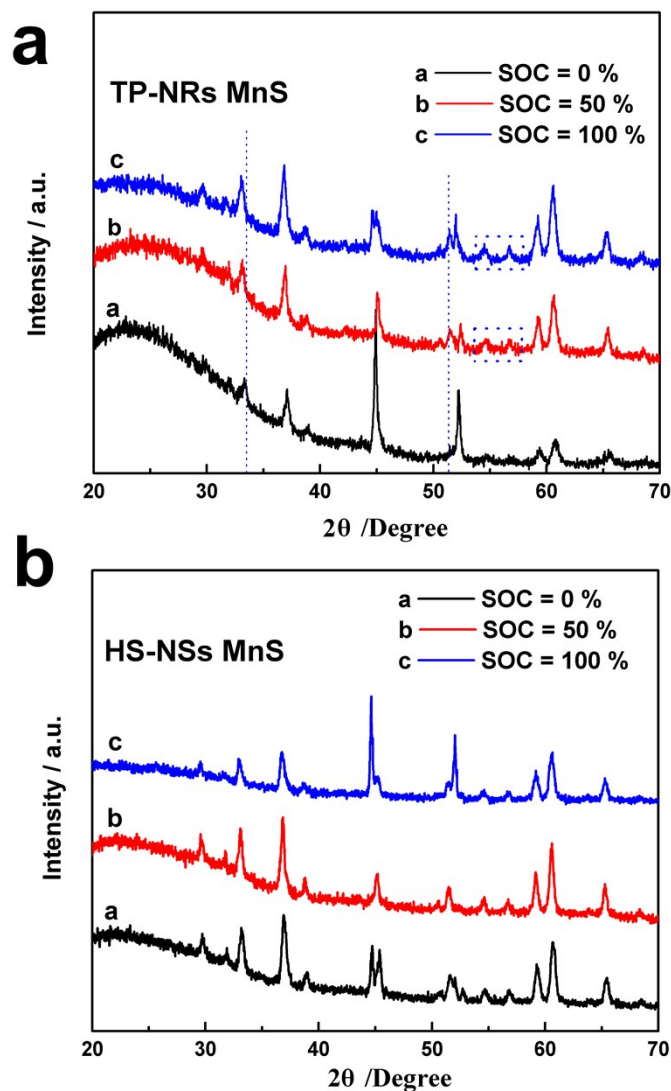


Figure S4. XRD patterns of the TP-NRs (a) and HS-NSs (b) MnS nanocrystals at different state of charges (SOC).

Discussion: As shown in the **Figure S4a**, when the TP-NRs MnS electrode is charged to 50% and 100%, negative shift of the peaks at 33° (left dotted line), corresponding to the expand of lattice, demonstrates the intercalation of hydroxyl into the layered structure of the γ -phase MnS nanorods. The added peaks at 52°, 55° and 57° (dotted line and dashed box) in the XRD patterns of TP-NRs MnS electrode at the SOC of 50% and 100% should be attributed to the phase change caused by the intercalation of hydroxyl. For comparison, only few changes are observed in the XRD patterns of HS-

NSs MnS electrode at different SOC (**Figure S4b**). These results confirm that the higher specific capacitance of TP-NRs MnS electrode is ascribed to the intercalation of hydroxyl into the layered structure of the γ -phase MnS nanorods, which contributes the pseudocapacitance of the TP-NRs MnS material (**Figure 3e**).

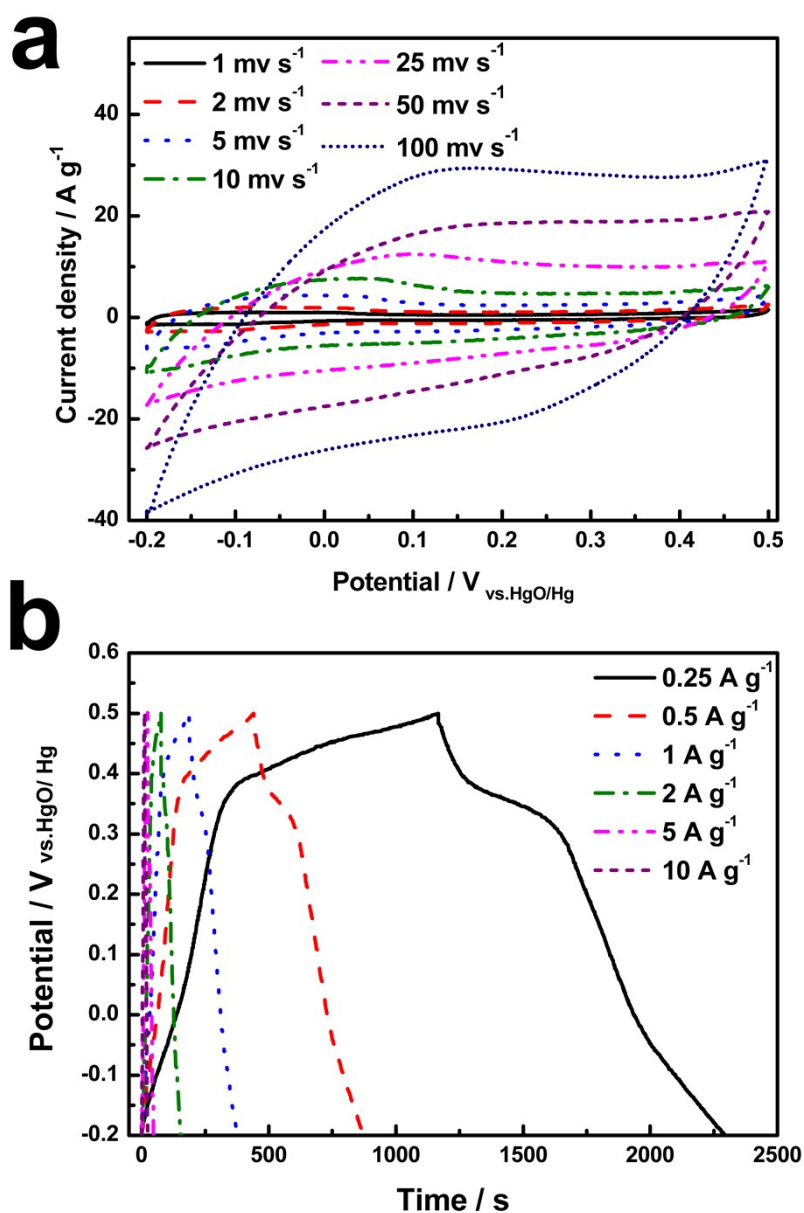


Figure S5. CV curves at different scan rates (a) and charge-discharge curves at different current densities (b) of TP-NRs nanocrystals in the 2.0 M KOH solution.

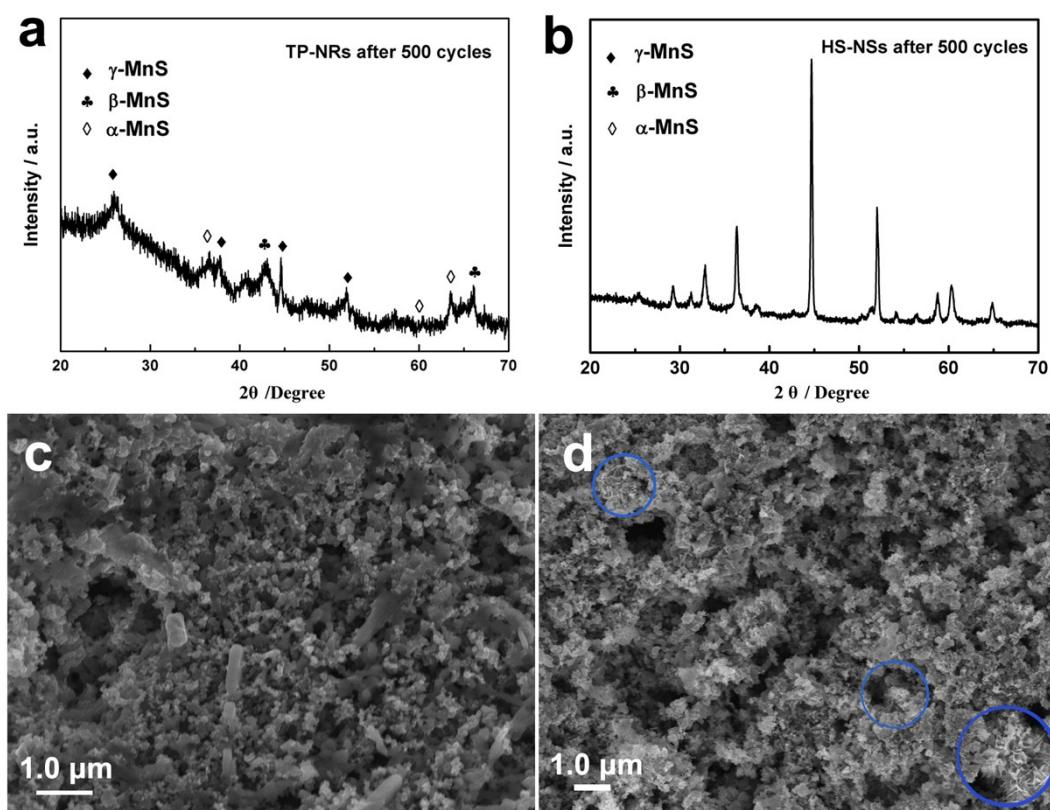


Figure S6. XRD patterns of TP-NRs (a) and HS-NSs (b) MnS nanocrystals after 500 charge-discharge cycles, SEM images of TP-NRs (c) and HS-NSs (d) MnS nanocrystals after 500 charge-discharge cycles

Discussion: As shown in **Figure S6a**, after 500 charge-discharge cycles, more stable α -phase MnS is present in the TP-NRs MnS sample. For comparison, there is little change for the HS-NSs MnS sample after 500 charge-discharge cycles (**Figure S6b**). These results indicate that the degradation of MnS electrodes should be attributed to the phase-transfer of MnS nanocrystals. Moreover, it is confirmed that the higher specific capacitance of TP-NRs MnS electrode than that of HS-NSs MnS electrode should be ascribed to the intercalation of hydroxyl into the layered structure of the γ -phase MnS nanorods, which contributes the pseudocapacitance of the materials. However, the intercalation/deintercalation of hydroxyl ion may cause the phase-

transfer of the metastable γ -phase MnS nanocrystals. The SEM images of the TP-NRs and HS-NSs MnS samples after 500 charge-discharge cycles are shown in **Figure S6c** and **S6d**, respectively. As shown, the nanorods are still observed after charge-discharge cycles although the tetrapod structure is collapsed. For comparison, flower-like nanoflakes (labeled by blue circles) are present in the HS-NSs MnS sample after 500 charge-discharge cycles.

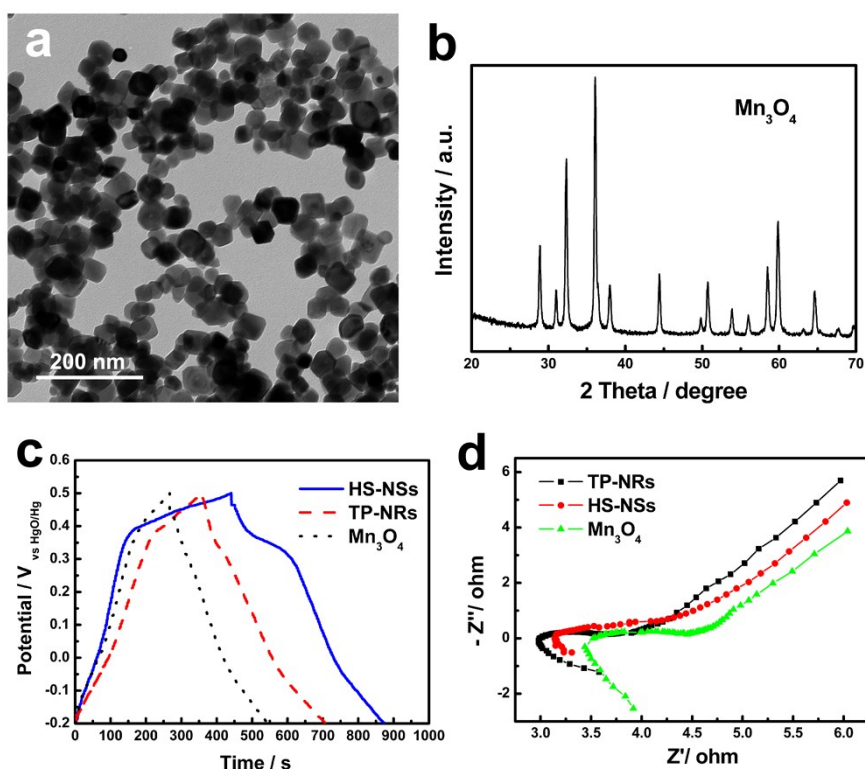


Figure S7. (a) TEM image and (b) XRD pattern of Mn_3O_4 nanocrystals obtained from calcining the $\text{Mn}(\text{OH})_2$ (shown in **Figure S1c** and **S1d**) at $400\text{ }^\circ\text{C}$ for 2 h. (c) charge-discharge curves for the comparison between MnS nanocrystals electrodes and Mn_3O_4 nanocrystals electrode in 2.0 M KOH solution (d) EIS spectra of MnS TP-NRs, MnS HS-NSs and Mn_3O_4 nanocrystals electrodes.

Discussion: As shown in **Figure S7a**, the spindle-like morphology is kept after $400\text{ }^\circ\text{C}$ calcining for $\text{Mn}(\text{OH})_2$ nanocrystals, which should be transferred into manganese oxide. The XRD pattern indicates that the manganese oxide is spinel manganese oxide

Mn_3O_4 (Figure S7b), which is widely used as supercapacitor materials. As shown in Figure S7c, both the TP-NRs and the HS-NSs MnS nanocrystals electrodes, which are primary used in supercapacitor, exhibit higher specific capacitance than the spinel Mn_3O_4 electrode. It can be attributed to the better electronic conductivity of transition metal sulfide than that of corresponding metal oxide, as well as fast charge transfer process. As shown in the EIS spectra of the three electrodes (Figure S7d), both the ohmic resistance and charge transfer resistance of Mn_3O_4 electrode are higher than those of both MnS TP-NRs and HS-NSs electrodes, indicating the better electronic conductivity and electrochemical reaction activity of MnS nanocrystals than manganese oxides. Moreover, the specific capacitance of MnS nanocrystals electrodes are higher than that of manganese oxides reported in literatures [1-2].

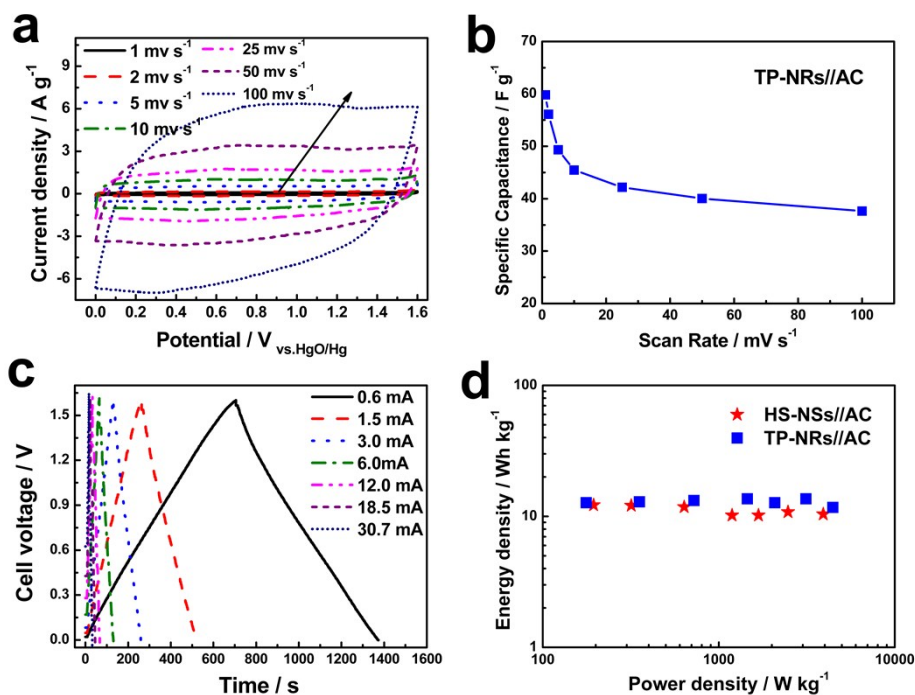


Fig. S8 (a) CV curves at different scan rates and (b) specific capacitances at different scan rates of the as-prepared TP-NRs//AC supercapacitor, (c) Charge-discharge curves of TP-NRs//AC

supercapacitor at different current in 2.0 M KOH electrolyte (d) Ragone plots (energy density versus power density) of the as-prepared HS-NSs//AC and TP-NRs//AC supercapacitors

Reference

- [1] S. Santhanagopalan, A. Balram, D. D. Meng, *ACS Nano* **2013**, 7, 2114-2125.
- [2] H. Zhang, G. Cao, Z. Wang, Y. Yang, Z. Shi, Z. Gu, *Nano Lett.* **2008**, 8, 2664-2668.